



Universiteit
Leiden
The Netherlands

Impact of region of interest definition on visual stimulation-based cerebral vascular reactivity functional MRI with a special focus on applications in cerebral amyloid angiopathy

Harten, T.W. van; Rooden, S. van; Koemans, E.A.; Opstal, A.M. van; Greenberg, S.M.; Grond, J. van der; ... ; Osch, M.J.P. van

Citation


Harten, T. W. van, Rooden, S. van, Koemans, E. A., Opstal, A. M. van, Greenberg, S. M., Grond, J. van der, ... Osch, M. J. P. van. (2023). Impact of region of interest definition on visual stimulation-based cerebral vascular reactivity functional MRI with a special focus on applications in cerebral amyloid angiopathy. *Nmr In Biomedicine*, 36(7).
doi:10.1002/nbm.4916

Version: Publisher's Version
License: [Creative Commons CC BY 4.0 license](#)
Downloaded from: <https://hdl.handle.net/1887/3748057>

Note: To cite this publication please use the final published version (if applicable).

RESEARCH ARTICLE

Impact of region of interest definition on visual stimulation-based cerebral vascular reactivity functional MRI with a special focus on applications in cerebral amyloid angiopathy

Thijs W. van Harten¹  | Sanneke van Rooden¹ | Emma A. Koemans² |
Anna M. van Opstal¹ | Steven M. Greenberg³ | Jeroen van der Grond¹ |
Marieke J. H. Wermer² | Matthias J. P. van Osch¹

¹Department of Radiology, Leiden University Medical Center, Leiden, The Netherlands

²Department of Neurology, Leiden University Medical Center, Leiden, The Netherlands

³Department of Neurology, Massachusetts General Hospital, Boston, Massachusetts, USA

Correspondence

Thijs W. van Harten, Leiden University Medical Center, PO Box 9600, Postal zone C3-Q, 2300 RC Leiden, The Netherlands.

Email: t.w.van_harten@lumc.nl

Funding information

Dutch Research Council (NWO), Grant/Award Number: 14729; Dutch Heart Foundation to M.J.H. Wermer, Grant/Award Number: 2016T86

Abstract

Cerebral vascular reactivity quantified using blood oxygen level-dependent functional MRI in conjunction with a visual stimulus has been proven to be a potent and early marker for cerebral amyloid angiopathy. This work investigates the influence of different postprocessing methods on the outcome of such vascular reactivity measurements. Three methods for defining the region of interest (ROI) over which the reactivity is measured are investigated: structural (transformed V1), functional (template based on the activation of a subset of subjects), and percentile (11.5 cm³ most responding voxels). Evaluation is performed both in a test-retest experiment in healthy volunteers (N = 12), as well as in 27 Dutch-type cerebral amyloid angiopathy patients and 33 age- and sex-matched control subjects. The results show that the three methods select a different subset of voxels, although all three lead to similar outcome measures in healthy subjects. However, in (severe) pathology, the percentile method leads to higher reactivity measures than the other two, due to circular analysis or “double dipping” by defining a subject-specific ROI based on the strongest responses within each subject. Furthermore, while different voxels are included in the presence of lesions, this does not necessarily result in different outcome measures. In conclusion, to avoid bias created by the method, either a structural or a functional method is recommended. Both of these methods provide similar reactivity measures, although the functional ROI appears to be less reproducible between studies, because slightly different subsets of voxels were found to be included. On the other hand, the functional method did include fewer lesion voxels than the structural method.

KEYWORDS

cerebral amyloid angiopathy, cerebral vascular reactivity, functional MRI, postprocessing

Abbreviations used: AMP, amplitude; BOLD, blood oxygen level-dependent; CAA, cerebral amyloid angiopathy; D-CAA, Dutch-type cerebral amyloid angiopathy; EDAN, Early Detection Angiopathy Network; HRF, hemodynamic response function; ICH, intracerebral hemorrhage; ROI, region of interest; SWI, susceptibility-weighted image; TE, echo time; TR, repetition time; TTB, time to baseline; TTP, time to peak.

This is an open access article under the terms of the [Creative Commons Attribution](https://creativecommons.org/licenses/by/4.0/) License, which permits use, distribution and reproduction in any medium, provided the original work is properly cited.

© 2023 The Authors. *NMR in Biomedicine* published by John Wiley & Sons Ltd.

1 | INTRODUCTION

Cerebral vascular reactivity functional MRI (fMRI), the vascular response to a stimulus, is an increasingly recognized marker for several brain diseases.¹⁻³ One of these diseases is sporadic cerebral amyloid angiopathy (CAA), a major cause of intracerebral hemorrhages (ICHs) and cognitive decline in the elderly.⁴⁻⁶ In CAA, the protein amyloid-beta accumulates in the vessel wall of leptomeningeal arteries. The current diagnosis of CAA focuses primarily on clinical symptoms combined with hemorrhagic hallmarks on MRI.^{7,8} However, a multitude of ischemic processes are also observed: there is a strong association with cortical thinning,^{9,10} white matter hyperintensities, microinfarcts,¹¹ and changes in diffusion tensor measures.¹² Moreover, impaired cerebrovascular function has been proven to be an important hallmark.¹³⁻¹⁶ More specifically, in patients with Dutch-type hereditary CAA (D-CAA, also known as hereditary cerebral hemorrhage with amyloidosis - Dutch type [or HCHWA-D]), vascular reactivity has been found to be an early marker (i.e., already showing differences compared with age-matched controls in mutation carriers without prior ICH).¹⁷ Moreover, reactivity decreased over time in (D-)CAA patients, in contrast to healthy controls.^{13,18,19} Therefore, vascular reactivity can be considered a promising marker to monitor CAA progression over time, for example, as an outcome measure in clinical trials.

When measuring vascular reactivity, both the readout as well as the challenge need to be chosen. Blood oxygen level-dependent (BOLD) fMRI is considered to be a powerful readout to facilitate the quantification of vascular reactivity. The BOLD fMRI signal is, however, a very complicated type of contrast, believed to be a combination of changes in oxygen consumption, regional blood flow, and regional blood volume. To map full brain vascular reactivity with MRI, the most commonly used challenges are CO₂-based approaches, such as carbogen breathing or breath-hold experiments, or less commonly administration of acetazolamide.²⁰ Previous works in CO₂-based approaches in CAA found a diminished vascular reactivity as measured by BOLD fMRI, with a stronger preference in the occipital region of the brain.²¹ Furthermore, while evoked potentials remained unchanged, the BOLD response was affected in CAA patients, suggesting a more important contribution of vascular reactivity than neuronal activity in the observed BOLD changes.²²

To measure vasoreactivity in the field of CAA, most studies employ a visual stimulus and monitor the hemodynamic response to that stimulus in the visual cortex via BOLD fMRI.^{13-15,17-19,23} This relatively simple approach is chosen because CAA pathology appears to have an occipital preference, the robustness of the visual cortex' hemodynamic response to this stimulus and the noninvasive nature of the administration of such a stimulus. As the small penetrating arteries in the brain are affected in CAA, the changes in BOLD signal change are hypothesized as a surrogate marker for vascular reactivity for subsequent quantification. In such fMRI experiments a region of interest (ROI) is determined containing voxels within the activated region and, subsequently, response characteristics, such as the amplitude, time to peak, and time to baseline, are used as outcome measures. However, little consistency exists in the literature on how to define this ROI, whereas measures like the amplitude are crucially dependent on such a definition. Roughly two categories of ROI definitions can be discerned: anatomical and functional. Anatomical ROI definitions rely on atlas-based or group-wise defined ROIs that are registered onto the BOLD-scan of a subject for extraction of the response signals. Functional ROI definitions rely on a two-step approach: in the first step it is determined what voxels are activated by the stimulus and, subsequently, in the second step, the ROI is created based upon all or a subset (like the maximally activated voxels) of the activated voxels.

When considering the use of vascular reactivity as an outcome marker for clinical treatment studies in CAA²⁴ it is important to recognize that consistent ROI definitions are essential. When used in patients, the presence of pathology, like hemorrhages in CAA, can be expected and the ROI definition should be able to deal with these (i.e., still provide accurate estimation of the vascular reactivity markers). This might limit the potential of atlas-based ROI definitions, especially when taking into account that activated regions may be shifted outside of the area defined by an atlas that is constructed based on the data of healthy subjects. However, functional definitions might be affected by circular analysis, or "double dipping", especially when the ROI is defined at the individual level: first the level of activation is determined, and subsequently the amplitude (or timing) of the maximally (or significantly) affected voxels is determined (i.e., selection of voxels is directly or indirectly based upon the outcome marker one is interested in).

In this work three methods for ROI definition and the influence of this definition on outcome markers are investigated. Evaluation is carried out by four experiments with the first three performed on a reproducibility dataset in healthy volunteers and the last performed in presymptomatic and symptomatic D-CAA patients. In the first experiment, the ROIs resulting from each of the methods were compared in volume and overlap (described in subsection 2.5.1). In the second experiment, the outcome measures generated by each of the ROIs were compared (described in subsection 2.5.2). In the third experiment, the effects on reproducibility of ROI generation and outcome measures were compared (described in subsection 2.5.3). And in the fourth experiment, the impact of the presence of lesions within the visual cortex was investigated for the different approaches (described in subsection 2.5.4).

2 | METHODS

To fully explore all of the aforementioned aspects two distinct datasets were analyzed: one dataset with DNA-proven D-CAA mutation carriers and age- and sex-matched control subjects, in which the influence of pathology was studied; and one with strictly healthy participants who were scanned twice, with ~3 weeks between sessions, to allow assessment of reproducibility.¹⁸ The D-CAA patient-control dataset was acquired with

the same scan parameters and on the same MR scanner as used for the healthy subjects. This D-CAA dataset has been previously described and was acquired as part of the study Early Detection of Angiopathy Network (EDAN).¹⁷ Patient characteristics are summarized in Table 1. Informed consent was obtained from all participants of both cohorts. In line with institutional review board (IRB) regulations, formal IRB approval was waived for the cohort of healthy participants, and study protocols for the D-CAA patient-control dataset were approved by the local IRB.

2.1 | MRI acquisition

All participants were scanned on a whole-body Philips Achieva 3-T MRI system (Best, The Netherlands) using a 32-channel head coil. Structural 3D T1-weighted (T1-W) images (echo time [TE] 4.6 ms, repetition time [TR] 9 ms, flip angle 8°, field of view [FOV] = 224 × 177 × 168 mm, scan duration ~5 min); a 3D T2*-weighted image with a TE/TR of 31/45 ms, FOV 250 × 175 × 112 mm, matrix 320 × 317, 114 slices, and scan duration of 155 s; and BOLD fMRI scans were acquired with a TE/TR of 31/1499 ms, FOV 220 × 220 × 75 mm, matrix 80 × 80, 25 slices, 130 dynamics, scan duration 201 s repeated three times. The visual stimulus consisted of 12 blocks of an 8-Hz flashing radial black-and-white checkerboard pattern for 20 s alternated with 28 s of a fixed gray screen as the rest condition.^{14,17}

2.2 | Preprocessing

2.2.1 | Anatomical scans

Anatomical scans were processed using tools available in FSL v. 6.0 (FMRIB's Software Library, www.fmrib.ox.ac.uk/fsl). First, nonbrain tissue was removed using the Brain Extraction Tool (BET). The T1-W scans were segmented using FMRIB's Automated Segmentation Tool (FAST)²⁵ and the white matter borders were used for a boundary-based linear coregistration with the fMRI scans²⁶ as contained in FLIRT.^{27,28} Then the structural scans were registered to the standard MNI152 template contained in FSL (MNI152NLIN6Asym) using first linear (FLIRT^{27,28}) and subsequently nonlinear registration (FNIRT²⁹). The inverses of these matrices were later applied to transform atlases to the participant's T1-W and subsequently to their fMRI scans.

2.2.2 | Functional scans

fMRI data processing was carried out using FEAT (the FMRI Expert Analysis Tool) version 6.00, which is part of FSL. The following prestatistics processing were applied: motion correction using MCFLIRT²⁷; slice-timing correction using Fourier-space time-series phase-shifting; nonbrain removal using BET³⁰; spatial smoothing using a Gaussian kernel of full width at half maximum 3.0 mm; grand-mean intensity normalization of the entire 4D dataset by a single multiplicative factor; and high-pass temporal filtering (Gaussian-weighted least-squares straight line fitting, with sigma = 24.0 s). To investigate the possible presence of unexpected artefacts or activation, independent component analysis-based exploratory data analysis was carried out using MELODIC.³¹ The statistical analysis of the time-series was carried out using FILM with local autocorrelation correction.³² The obtained z-statistic map was used for further analysis.

2.3 | ROI determination

To investigate the impact of ROI determination on outcome measures, three previously proposed approaches were compared, each of which is described below.

TABLE 1 Participant characteristics

	HEALTHY	CLINICAL STUDY (EDAN)		
		PRESYMPTOMATIC	SYMPTOMATIC	CONTROLS
Age (years)	42 ± 12	34 ± 12	55 ± 5	46 ± 14
Sex				
Men	10 (83%)	3 (25%)	7 (47%)	13 (39%)
Women	2 (17%)	9 (75%)	8 (53%)	20 (61%)

Abbreviation: EDAN, Early Detection Angiopathy Network.

2.3.1 | “Structural” ROI

One way of defining the ROI over which the hemodynamic response is averaged is to transform the standardized atlas of the visual cortex to the subject's fMRI space. A previous study applied this method of deriving an ROI as a secondary analysis.¹³ From the Juelich atlas,³³ the V1 visual cortex was selected and transformed from MNI to structural space and subsequently to functional space using the linear and nonlinear transformations from the earlier described registration.^{26–29} This method is referred to as the “structural” method.

2.3.2 | Group-based “functional” ROI

In other studies, a group-based functional ROI was determined based on group-based activation in a subset of the participants.^{14,17} In short, z-statistic maps of the included participants were transformed to a standard cortical ribbon (fsaverage from FreeSurfer).³⁴ Mean activation was determined using a one-sample group mean GLM and a contiguous region of activation was created by applying an uncorrected significance threshold of p less than 0.001. This ROI was then transformed back to the individual fMRI spaces. The procedure is described in detail in Dumas et al.¹⁴ In our study, for each dataset we generated a separate functional ROI: for the first datasets (healthy subjects) two separate functional ROIs were created for the first and second visit; for the second (EDAN) dataset, a single functional ROI was created based on the first eight D-CAA mutation carriers and their eight age- and sex-matched control subjects, resulting in a template based on 16 participants. This method will be referred to as the “functional” method.

2.3.3 | Activation ROI: “percentile” of z-statistics map

The third proposed method selects an individual ROI based on the participant's z-statistic map.^{13,18,19,35} For each individual, the top percentile or predetermined volume of voxels with the highest z-score is selected as the ROI. In this study, we included a region with a volume of 11.5 cm³, containing the 503 most active voxels.¹³ This method is referred to as the “percentile” method.

2.4 | Hemodynamic response function models

A further consideration is the hemodynamic response function (HRF), or basis function, to be convoluted with the stimulus profile in the analysis.²³ Using different HRF models as the basis function may yield different results in the functional- and activation-based approaches. Therefore, both a gamma and an “optimal” HRF generated by FSL's FMRIB Linear Optimal Basis Sets (FLOBS) are investigated in this study.³⁶ Results of these analyses are presented in the supporting information. When not mentioned explicitly, data were analyzed with the gamma HRF.

2.5 | Comparing ROI methods

The three approaches for defining the ROI were compared both at the ROI level (i.e., overlap and total volume of the ROI), as well as at the outcome level (amplitude and timing parameters of the BOLD response). First, ROIs were generated using the aforementioned methods for all subjects. The average time course of the BOLD response to the visual stimulus for each study participant was calculated by averaging the time-courses of all voxels within the ROI and converting to BOLD percentage signal change using the time-course average as baseline value, then averaging across all stimulus blocks. The block responses were subsequently fitted to a trapezoidal function defined by three parameters: the time to reach peak (TTP) response, the response amplitude (AMP), and the time to return to baseline (TTB) using a previously described fitting algorithm.^{14,17}

2.5.1 | Comparison at the ROI level

To assess to what extent the three approaches result in a similar ROI, the Dice coefficient (see Equation 1: area of the overlapping voxels divided by the sum of the areas of both ROIs) was assessed between all ROIs³⁷:

$$Dice = \frac{2 * (|ROI_{method 1} \cap ROI_{method 2}|)}{|ROI_{method 1}| + |ROI_{method 2}|} \quad (1)$$

2.5.2 | Comparison at the outcome level

Subsequently, the approaches were compared by testing the impact of the ROI selection on the ROI-averaged primary outcome measures (TTP, TTB, and AMP) using correlation and Bland–Altman plots. Group differences were assessed using a regression model, adjusting for age and sex, between presymptomatic mutation carriers and controls, as well as between symptomatic mutation carriers and controls.

2.5.3 | Comparison of reproducibility

The datasets of healthy participants were tested for reproducibility of both the ROIs and outcome measures. Intrasubject intersession ROIs were tested for each method using the Dice coefficient, and outcome measures were tested for reproducibility by calculating the Pearson correlation between sessions.³⁸

2.5.4 | Assessment of the influence of lesions

As already mentioned, a complicating matter when measuring the vascular response in neurovascular patients is the presence of pathological tissue and imaging artifacts due to cerebral hemorrhages. It is important to note is that these are much more prevalent in D-CAA than in sporadic CAA patients and different studies deal with them differently. Some opt, for example, to disregard the complete hemisphere when an ICH is present, while others exclude ICHs based on manual delineation of lesions. To test the influence of the presence of lesions, a similar approach as described in Dumas et al.¹⁴ (described in detail in their supplemental material) was used: the BOLD scans were coregistered with T2*-weighted images and hemorrhagic lesions were manually masked out on the BOLD scan by an experienced rater (E.K., 5 years of experience); furthermore, these masks were isotropically dilated by 7 mm to provide more rigorous masks. All voxels within these masks were then subsequently excluded from the secondary analysis. Relative remaining volumes were determined both when excluding only voxels with presence of hemosiderin, as well as with the dilated lesion mask. Outcome measures were assessed again for all participants.

3 | RESULTS

3.1 | Comparison at the ROI level

Visual inspection showed that the different methods resulted in different ROI selections, with the biggest difference in the number of voxels included, whereas for all methods most of the selected voxels were located in the occipital lobe, as expected for a visual paradigm (Figure 1). However, in symptomatic patients, many spurious voxels were observed, spread throughout the whole brain, when ROI selection was based upon the percentile method (an example is shown in Figure 1L). An example of the effect of using a different HRF is shown in Figure S1. When quantified using the Dice coefficient, it became clear that the three methods resulted in quite different selections (Table 2). The highest Dice coefficient (with a maximum value of 0.255 in the healthy cohort) was found between the ROIs based on the group-based functional activations and the ROIs with the highest 11.5 cm³ responding voxels of the z-statistic map. The overlap between the ROIs of the different methods was smaller in the dataset of the clinical study compared with the dataset of healthy subjects.

3.2 | Comparison at the outcome level

Our analysis of the data from the clinical EDAN study is provided in Figure 2, showing that the ROI-selection method would have impacted the conclusion from a between-group comparison. In particular, when using the percentile method, no difference between the younger and older control participants was observed, whereas for the other two methods the older control subjects showed a smaller amplitude. Moreover, a clearer response was observed for the percentile method in the symptomatic patients than for the other two methods (Figure 2). Mean group BOLD responses when using a different HRF are shown in Figure S2.

Figure 3 shows two Bland–Altman plots illustrating two typical findings as also observed in many of the other Bland–Altman plots (all the Bland–Altman plots can be found in Figure S3). First, a large variation in differences in timing parameters was observed for higher values of the timing parameters, especially between the structural and functional methods (the right part of the Bland–Altman plot). Second, a proportional error with significant bias was found when the amplitude outcome measure of the percentile ROI method was compared with either the functional or structural method. Furthermore, group averages for outcome measures are shown in Table 3; differences between mutation carriers and control subjects were assessed with a regression model, adjusting for age and sex. While trends appear to be relatively stable between the

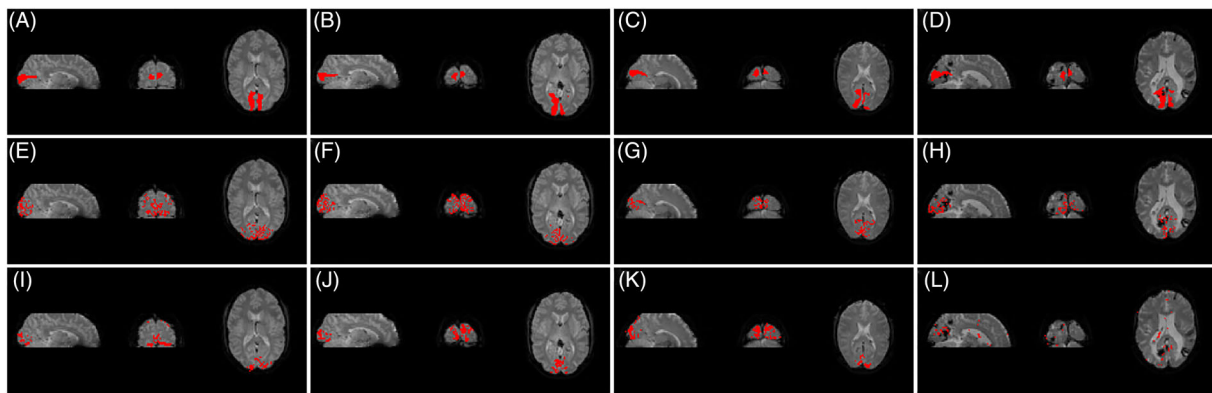


FIGURE 1 ROIs as determined by the different methods: the first row (A-D) shows the structural method based on the registration of an atlas-based V1 ROI to the subject-space; the second row (E-H) depicts the functional ROI based upon an group-averaged activation map, and the final row (I-L) shows the percentile method that selects for each subject the strongest responding voxels up to an ROI volume of 11.5 cm^3 . The first column (A,E,I) shows the first visit of a healthy subject, the second column (B,F,J) the second visit of the same healthy subject, the third column (C,G,K) shows a control subject of the EDAN study, and the final column (D,H,L) shows a symptomatic D-CAA mutation carrier. Clear differences can be observed between the ROIs selected by the different methods. Furthermore, it can be seen that, within the symptomatic mutation carrier, some methods include voxels in the ROI that are located within the ICH, and that with the z-statistic-based approach a more random pattern is obtained for the ROI, including many voxels not located within the occipital lobe. An example of the effect of using a different HRF is shown in Figure S1. D-CAA, Dutch-type cerebral amyloid angiopathy; EDAN, Early Detection Angiopathy Network; HRF, hemodynamic response function; ICH, intracerebral hemorrhage; ROI, region of interest

TABLE 2 Dice coefficient showing the overlap between ROIs obtained by different methods. All methods have a low level of overlapping voxels with one another

	Healthy			Clinical study (EDAN)		
	STRUCTURAL	FUNCTIONAL	PERCENTILE	STRUCTURAL	FUNCTIONAL	PERCENTILE
structural	-	0.177 ± 0.031	0.184 ± 0.040	-	0.190 ± 0.061	0.156 ± 0.066
functional	0.177 ± 0.031	-	0.255 ± 0.035	0.190 ± 0.061	-	0.196 ± 0.070
percentile	0.184 ± 0.040	0.255 ± 0.035	-	0.156 ± 0.066	0.196 ± 0.070	-

Abbreviations: EDAN, Early Detection Angiopathy Network; ROI, region of interest.

structural and functional methods, TTP in particular seems to yield different results when using the percentile method: the presymptomatic group is no longer significantly different from control participants, and symptomatic patients have a TTP much closer to control subjects as well.

3.3 | Comparison of reproducibility

When comparing the outcome measures on vascular reactivity between two repeated measurements (~ 3 weeks apart), good reproducibility was found for all three ROI-selection approaches; see Table 4, which shows the Pearson correlation coefficients and p values. When comparing the three outcome measures, TTB was less reproducible than the other two outcome measures. When comparing the three ROI-selection methods, the functional ROI approach performed slightly poorer than the other two methods (Table 4).

3.4 | Assessment of the influence of lesions

Figure 4 shows an example of a patient with a hemorrhage in the visual cortex. All three ROI selection algorithms resulted in inclusion of voxels located within the hemorrhagic lesion, which was outlined on a coregistered susceptibility-weighted image (SWI) sequence. While the functional and structural methods showed a similar number of voxels within the ICH (15.7% and 17.1%, respectively), the ROI obtained by the percentile method contained fewer voxels within or near the lesions. The fraction of voxels remaining after exclusion of hemorrhagic lesions and when using a dilated lesion mask is shown in Figure S4.

At group level, the exclusion of hemorrhagic voxels, both with and without dilation of the ROIs, appears to have only a minor impact upon outcome measures.

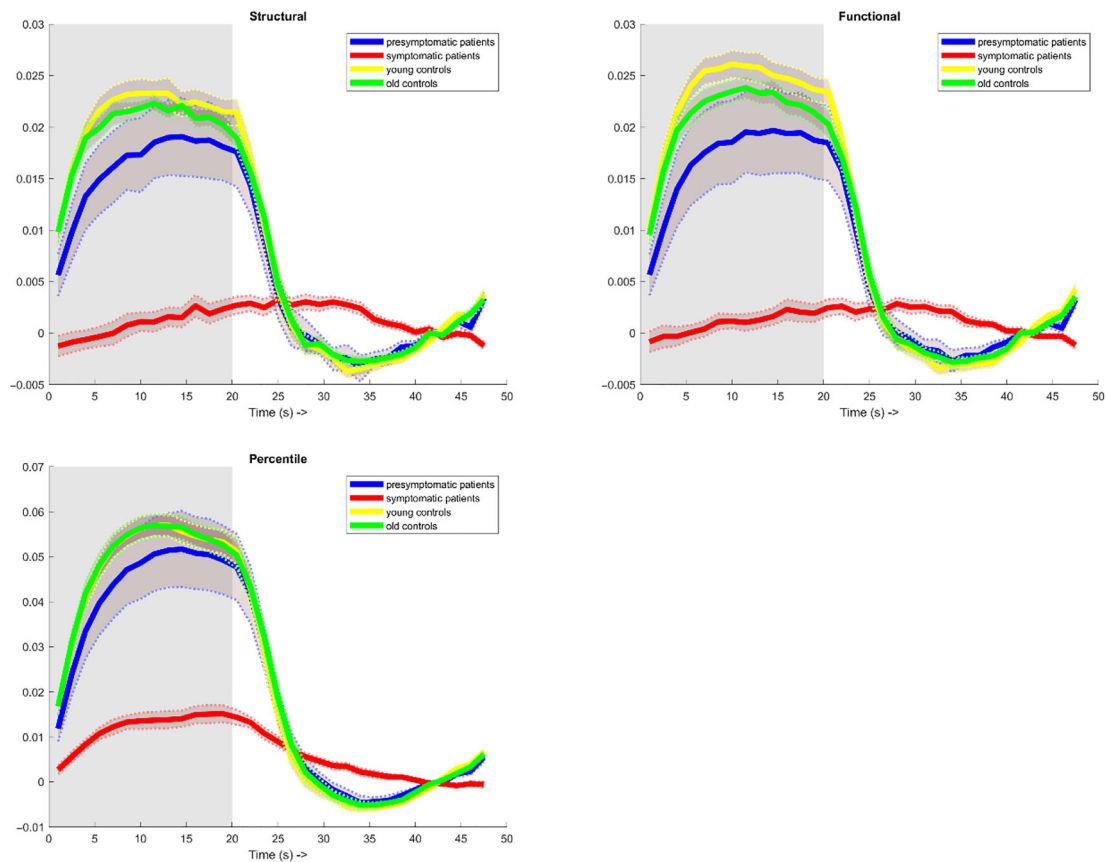


FIGURE 2 Group averages (solid lines) and standard error of the mean (dashed lines) when applying the different methods for the ROI definition over which the BOLD response upon visual stimulation is determined. In order (left to right, top to bottom): the different methods for ROI definition, respectively, structural, functional, and percentile. The blue curves show the average response in presymptomatic D-CAA patients ($N = 12$), the yellow curves show the averaged response in control subjects age-matched with the presymptomatic D-CAA carriers, the red curves show the response of symptomatic patients, and the green curves show the control subjects age-matched with the symptomatic D-CAA carriers. The structural and functional methods yield similar results, whereas the percentile method fails to pick up differences between young and old control subjects. Moreover, the amplitude of all curves of the percentile method is higher compared with the other two ROI-selection approaches and a more pronounced response is found in symptomatic D-CAA patients. BOLD, blood oxygen level-dependent; D-CAA, Dutch-type cerebral amyloid angiopathy; ROI, region of interest

4 | DISCUSSION

The findings of this study confirm that different ROI-selection approaches for calculating visual task-based vascular reactivity significantly affect the outcome: we showed that this results in different voxels included for analysis, that the inclusion of these voxels leads to different outcome measures, that it can affect trends as observed in group analyses, and that the impact of pathology on these outcome measures differs between the approaches.

When applying three previously proposed postprocessing methods, different ROIs are selected with only very moderate Dice overlap scores between them. This would not per definition lead to differences in outcome measures: for example, if these subsets of voxels are in fact part of a larger region with a similar response to the stimulus, one would still obtain similar outcome measures. However, this work showed that the different ROIs not only have little overlap, they also lead to differences in outcome measures (see Table 3). Furthermore, whereas all three methods also selected voxels within hemorrhagic lesions, as identified on a SWI, the impact of this as measured by the percentage of selected voxels within or just outside the ICH-mask was much lower for one approach, the percentile method, compared with the other two methods. However, exclusion of ICH-voxels from the ROIs only had a small effect on the outcome measures.

These findings point to a dependency on the ROI-selection approach, but it is more difficult to decide on the best approach. Visual inspection of the ROIs selected in symptomatic D-CAA patients by the percentile method points to the intrinsic vulnerability of the approach towards circular analysis, or double dipping. In these symptomatic D-CAA patients, the vascular response to a visual stimulus as measured by BOLD is very low, or on average even close to being absent.¹⁷ Because of this almost absence of a BOLD response in the visual cortex, selection of voxels with the highest z-score resulted in the inclusion of many voxels outside of the occipital cortex, which probably by chance showed some correlation with the stimulus. While these voxels are very low in their z-score, the probability that the signal fluctuation found in these voxels is representative of

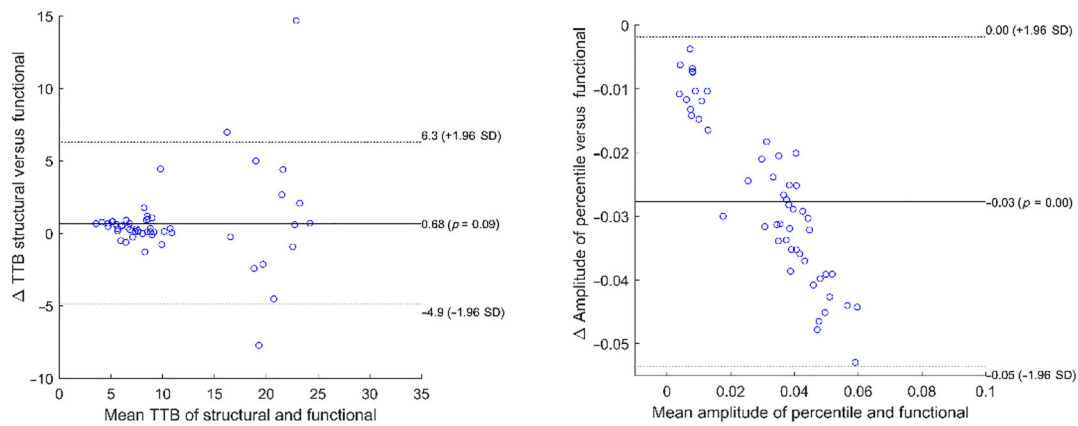


FIGURE 3 Two example Bland–Altman plots comparing different ROI selection approaches and their influence on the different outcome parameters. All the other Bland–Altman plots are shown in Figure S3. The left plot shows how comparable the TTB is when using the structural or functional method. The right plot compares the influence of ROI selection (percentile vs. functional method) on the amplitude of the visual reactivity. All Bland–Altman plots have been calculated on the data of the clinical study on D-CAA. Two main observations can be made. First, the variation between the TTB obtained with the structural and functional methods is highly dependent on the magnitude of the TTB, showing increased discordance between the methods for higher TTB values (left plot). Second, for the amplitude parameter, a proportional error in combination with significant bias can be observed (right plot) when comparing the percentile with the functional method. D-CAA, Dutch-type cerebral amyloid angiopathy; ROI, region of interest; TTB, time to baseline

TABLE 3 Mean time to peak, time to baseline, and amplitude outcome measures for each method, for presymptomatic mutation carriers, symptomatic mutation carriers, and control subjects. In brackets, the beta coefficient is reported. All values are reported with standard deviation, significantly different from control subjects at * $p < 0.05$, ** $p < 0.01$, *** $p < 0.001$; ^x indicates a significant result when correcting for multiple comparison using Bonferroni

		STRUCTURAL	FUNCTIONAL	PERCENTILE
Time to peak	Controls	4.95 ± 1.94	4.70 ± 1.62	6.29 ± 2.07
	Presymptomatic	9.83 ± 8.39 (0.505)** ^x	8.68 ± 7.54 (0.461)** ^x	7.16 ± 1.59 (0.194)
	Symptomatic	17.57 ± 10.48 (0.743)*** ^x	26.64 ± 14.54 (0.821)*** ^x	7.70 ± 2.81 (0.337)*
Time to baseline	Controls	7.23 ± 1.78	7.02 ± 2.10	8.27 ± 1.69
	Presymptomatic	10.69 ± 7.51 (0.462)** ^x	10.25 ± 6.39 (0.393)*	9.60 ± 3.60 (0.362)*** ^x
	Symptomatic	18.47 ± 4.30 (0.907)*** ^x	20.94 ± 4.84 (0.900)*** ^x	16.85 ± 4.53 (0.798)*** ^x
Amplitude	Controls	2.37 ± 0.612	2.50 ± 0.53	5.84 ± 1.21
	Presymptomatic	1.87 ± 1.07 (−0.521)*** ^x	1.22 ± 0.49 (−0.559)*** ^x	4.94 ± 2.60 (−0.465)*** ^x
	Symptomatic	0.42 ± 0.23 (−0.757)*** ^x	0.33 ± 0.25 (−0.810)*** ^x	0.63 ± 0.18 (−0.799)*** ^x

TABLE 4 Pearson correlation between the two visits of the healthy participants for each method and each outcome measure. Pearson coefficients and p values are displayed with the highest Pearson coefficient depicted in bold

	Time to peak		Time to baseline		Amplitude	
	Pearson	p value	Pearson	p value	Pearson	p value
STRUCTURAL	0.737	0.006	0.623	0.030	0.801	0.002
FUNCTIONAL	0.726	0.007	0.486	0.109	0.796	0.002
PERCENTILE	0.648	0.023	0.680	0.015	0.855	0.000

a true vascular response to the visual stimulus is rather small. This can also be deduced from the fact that some of these voxels are even found in regions where no vessel or brain tissue is present (e.g., inside the lateral ventricles; Figure 1L). Therefore, it can be assumed that mainly voxels are included with a similar pattern in the noise/artifact profile rather than voxels with a true vascular response. When averaging these voxels, a trend towards a response can be deduced from the data, simply because we selected noise voxels correlating mildly with the stimulus paradigm: a clear example of a double-dipping error and inclusion bias. The fact that this method appears to also change average group measures leads to a note of caution when applying this method in patients with severely disturbed vascular reactivity (see the supplementary data in the supporting information). Even although this approach is very robust against the presence of lesions (i.e., it selected the lowest percentage of voxels from within the ICH regions; e.g., Figure S4), we would only advise the use of this approach in populations with normal or only relatively mildly impaired vascular

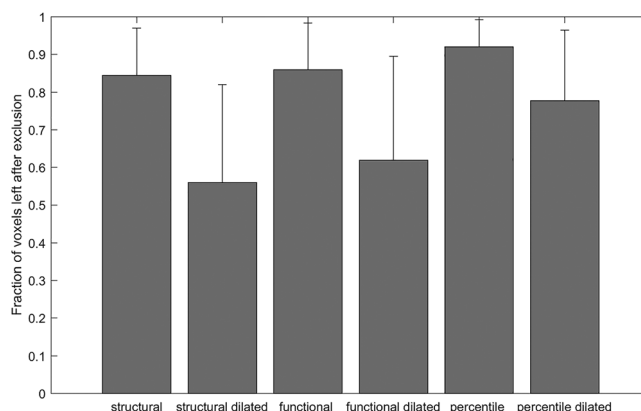


FIGURE 4 The bar graphs indicate the mean fraction of voxels remaining after excluding voxels within the ICH or after dilating the ICH segmentation with a 7-mm isotropic kernel. Error bars indicate standard deviation. For this graph only subjects who had one or more voxels were included. ICH, intracerebral hemorrhage

responses and thus not in symptomatic D-CAA patients. Furthermore, one could argue that an improved selection algorithm could easily be proposed by adding a constraint that only voxels in predetermined (posterior) parts of the brain are included. One would expect that such a hybrid method would also yield hybrid results, that is, a less pronounced hemodynamic response in mutation carriers than without such constraints, but more pronounced than the other methods. For this study, we decided to only include selection criteria that have been applied before, but hope that the results will stimulate proposals of new methods.

While for the structural and functional ROI determination the shape of the HRF has no to little impact, respectively, on the final results, there may be different voxels included when a different HRF is applied to the percentile approach. For example, we did notice a more visual cortex-based distribution in some (but not all) symptomatic D-CAA patients when using a different HRF (Figure S51). At a group level this did not lead to different results. However, further research should be conducted on how and why the HRF of these patients is changed.²³

Another note of caution is related to the influence of the ROI-selection procedure on the more extreme values of outcome measures. From the increased variance in the Bland-Altman plots for delayed timings (see, e.g., the right panel of Figure 3), it is clear that the selection process especially influences these measurements. Because of the very low response measured in the most affected patients, on one hand it becomes more arbitrary about which voxels to include, while on the other hand the inclusion of voxels with some response will have a more prominent influence on the mean shape of the response. In such cases, the fitted trapezoid may no longer be a good reflection of the real response, and whereas the amplitude might still reflect a correct measure (i.e., a small response), the timing parameters of the trapezoid may no longer be reflecting the true onset and recovery timings of the vascular response. Further research is needed into how to deal with such data. For example, abstaining from calculation of timing parameters for subjects in whom the amplitude of the response is below a certain threshold is one possible solution, whereas using a ceiling value on the timing parameters could be another.

Finally, it should be considered how to deal with pathology in patient studies. This is especially relevant in CAA patients, because ICH in the occipital lobe is a hallmark of the disease. In a previous study in sporadic CAA patients, a subanalysis was applied to exclude ICHs from the ROIs: a mask containing hemorrhagic lesions was made by an experienced observer based on a coregistered T2*-weighted sequence.¹⁴ This mask was subsequently dilated and those voxels were excluded from the secondary analysis. The exclusion of ICH-affected voxels was found to have little influence on the outcome markers. Another solution is the exclusion of the complete hemisphere from analysis when an ICH is present. Because ICH is even more prevalent in D-CAA compared with sporadic CAA, we did not exclude hemispheres in this study, nor in previous publications with this dataset.¹⁷ In our study we found differences in included voxels, at times ranging up to a reduction of up to 80% when using a dilated lesion mask. The number of voxels excluded by this method was smallest in the percentile method, as the chance that voxels in a hypointense region correlate with the visual stimulus paradigm is small. However, the impact on outcome measures was not significant. Furthermore, it should be noted that the processing time for the functional ROI approach was found to be much longer than for the other two methods, especially in the presence of cortical ICH, as each subject had to be processed by FreeSurfer.

There are some limitations to this study that need to be considered. First, we did not correct for confounding factors on the BOLD response such as heart rate and breathing that may influence the BOLD signal.^{39,40} Furthermore, there were no instructions for participants regarding diet, caffeine use, or other habits that may impact their vascular response. Another limitation is that the group-based functional method is based on a subset of the participants, as was done previously.^{14,17} This might have introduced a bias in the analysis. We did investigate whether using the second visit of the healthy participants or a different set of mutation carriers/healthy subjects would have led to significantly different ROIs. We observed a Dice coefficient of 0.75 for both experiments (data not shown), showing a large overlap and thus little influence on the ROI selection. Lastly, this study only looked at the effect of postprocessing. Different acquisition parameters, MRI hardware, paradigms, and trapezoidal fitting may also lead to different results. The strengths of our study are that the differences between currently applied models in this field of

research were not only tested in healthy subjects, but also in patients with different levels of vascular impairment. With the increasingly recognized importance of vascular reactivity measures in CAA research, our study aids in making informed choices on what approach to apply in future studies.

Our findings are limited to D-CAA patients, who have a much broader range of pathology than sporadic CAA patients, including the complete spectrum of presymptomatic patients up to patients with very severe pathology. Sporadic CAA patients are most frequently only diagnosed after entering the symptomatic phase, while frequently exhibiting a less severe form of pathology. On the other hand, sporadic CAA patients are on average older than the participants in our cohort, which may lead to additional confounding factors. However, in histopathology, as well as radiologically, the two are considered similar.^{41,42} Furthermore, when we compare vascular reactivity findings from D-CAA cohorts¹⁷ with findings from sporadic CAA patients,^{13,14} very similar changes can be observed. Therefore, we feel confident that the findings of this study on optimal postprocessing strategies can be directly translated to sporadic CAA.

Finally, it is important to recognize that these findings are not only relevant for studying neurovascular functioning in CAA, but also for other brain diseases, such as Alzheimer's disease, Huntington's disease, and CADASIL.^{35,43,44} With this broader application of such measures, it is increasingly important to create a more homogeneous approach for defining the ROI when performing these measurements.

In conclusion, to avoid the issue of circular analysis (double dipping), a transformed structural method or a functional method is recommended for neurovascular reactivity measurements. Both these methods appear to give similar results, with the structural method being more reproducible, whereas the functional method is more robust in the presence of hemorrhagic lesions in the occipital lobe. The poorer reproducibility of the functional method might be explained by interstudy changes of the mean activation mask, whereas a functional atlas exploits the same mask for all studies.

ACKNOWLEDGMENTS

This research has been made possible by the Dutch Heart Foundation and the Netherlands Organisation for Scientific Research (NWO), as part of their joint strategic research programme: "Earlier recognition of cardiovascular diseases". This project is partially financed by the PPP Allowance made available by Top Sector Life Sciences & Health to the Dutch Heart Foundation to stimulate public-private partnerships. This work is further supported by a grant of the Dutch Heart Foundation to M.J.H. Wermer (2016T86).

ORCID

Thijs W. van Harten  <https://orcid.org/0000-0002-3408-9379>

REFERENCES

- Smoliński Ł, Litwin T, Kruk K, Skowronska M, Kurkowska-Jastrzebska I, Czlonkowska A. Cerebrovascular reactivity and disease activity in relapsing-remitting multiple sclerosis. *Adv Clin Exp Med*. 2020;29(2):183-188. doi:10.17219/acem/114762
- Yeh MY, Chen HS, Hou P, et al. Cerebrovascular reactivity mapping using resting-state functional MRI in patients with gliomas. *J Magn Reson Imaging*. 2022;56(6):1863-1871. doi:10.1002/jmri.28194
- Thrippleton MJ, Shi Y, Blair G, et al. Cerebrovascular reactivity measurement in cerebral small vessel disease: Rationale and reproducibility of a protocol for MRI acquisition and image processing. *Int J Stroke*. 2018;13(2):195-206. doi:10.1177/1747493017730740
- Viswanathan A, Greenberg SM. Cerebral amyloid angiopathy in the elderly. *Ann Neurol*. 2011;70(6):871-880. doi:10.1002/ana.22516
- Boulouis G, Charidimou A, Greenberg SM. Sporadic cerebral amyloid angiopathy: pathophysiology, neuroimaging features, and clinical implications. *Semin Neurol*. 2016;36(3):233-243. doi:10.1055/s-0036-1581993
- Charidimou A, Boulouis G, Gurol ME, et al. Emerging concepts in sporadic cerebral amyloid angiopathy. *Brain*. 2017;140(7):1829-1850. doi:10.1093/brain/awx047
- Knudsen KA, Rosand J, Karluk D, Greenberg SM. Clinical diagnosis of cerebral amyloid angiopathy: validation of the Boston criteria. *Neurology*. 2001;56(4):537-539. doi:10.1212/WNL.56.4.537
- van Rooden S, van der Grond J, van den Boom R, et al. Descriptive analysis of the Boston criteria applied to a Dutch-type cerebral amyloid angiopathy population. *Stroke*. 2009;40(9):3022-3027. doi:10.1161/STROKEAHA.109.554378
- Fotiadis P, van Rooden S, van der Grond J, et al. Alzheimer's Disease Neuroimaging Initiative (ADNI) Cortical atrophy in patients with cerebral amyloid angiopathy: a case-control study. *Lancet Neurol*. 2016;15(8):811-819. doi:10.1016/S1474-4422(16)30030-8
- Subotic A, McCreary CR, Saad F, et al. Cortical thickness and its association with clinical cognitive and neuroimaging markers in cerebral amyloid angiopathy. *J Alzheimers Dis*. 2021;81(4):1663-1671. doi:10.3233/JAD-210138
- Wermer MJH, Greenberg SM. The growing clinical spectrum of cerebral amyloid angiopathy. *Curr Opin Neurol*. 2018;31(1):28-35. doi:10.1097/WCO.0000000000000510
- Reijmer YD, Fotiadis P, Charidimou A, et al. Relationship between white matter connectivity loss and cortical thinning in cerebral amyloid angiopathy. *Hum Brain Mapp*. 2017;38(7):3723-3731. doi:10.1002/hbm.23629
- Switzer AR, McCreary C, Batool S, et al. Longitudinal decrease in blood oxygenation level dependent response in cerebral amyloid angiopathy. *NeuroImage Clin*. 2016;11:461-467. doi:10.1016/j.nicl.2016.02.020
- Dumas A, Dierksen GA, Gurol ME, et al. Functional MRI detection of vascular reactivity in cerebral amyloid angiopathy. *Ann Neurol*. 2012;72(1):76-81. doi:10.1002/ana.23566
- Smith EE, Vijayappa M, Lima F, et al. Impaired visual evoked flow velocity response in cerebral amyloid angiopathy. *Neurology*. 2008;71(18):1424-1430. doi:10.1212/01.wnl.0000327887.64299.a4
- Nortley R, Korte N, Izquierdo P, et al. Amyloid β oligomers constrict human capillaries in Alzheimer's disease via signaling to pericytes. *Science*. 2019;365(6450):eaav9518. doi:10.1126/science.aav9518

17. van Opstal AM, van Rooden S, van Harten T, et al. Cerebrovascular function in pre-symptomatic and symptomatic individuals with hereditary cerebral amyloid angiopathy: a case-control study. *Lancet Neurol*. 2017;16(2):115-122. doi:10.1016/S1474-4422(16)30346-5
18. van Dijk SE, Lak J, Drenth N, et al. Aging effect, reproducibility, and test-retest reliability of a new cerebral amyloid angiopathy MRI severity marker-cerebrovascular reactivity to visual stimulation. *J Magn Reson Imaging*. 2023;57(3):909-915. doi:10.1002/jmri.28362
19. van Dijk SE, van der Grond J, Lak J, et al. Longitudinal progression of magnetic resonance imaging markers and cognition in Dutch-type hereditary cerebral amyloid angiopathy. *Stroke*. 2022;53(6):2006-2015. doi:10.1161/STROKEAHA.121.035826
20. Sleight E, Stringer MS, Marshall I, Wardlaw JM, Thrippleton MJ. Cerebrovascular reactivity measurement using magnetic resonance imaging: a systematic review. *Front Physiol*. 2021;12:643468. doi:10.3389/fphys.2021.643468
21. Beaudin AE, McCreary CR, Mazerolle EL, et al. Cerebrovascular reactivity across the entire brain in cerebral amyloid angiopathy. *Neurology*. 2022;98(17):e1716-e1728. doi:10.1212/WNL.000000000000200136
22. Peca S, McCreary CR, Donaldson E, et al. Neurovascular decoupling is associated with severity of cerebral amyloid angiopathy. *Neurology*. 2013;81(19):1659-1665. doi:10.1212/01.wnl.0000435291.49598.54
23. Williams RJ, Goodyear BG, Peca S, et al. Identification of neurovascular changes associated with cerebral amyloid angiopathy from subject-specific hemodynamic response functions. *J Cereb Blood Flow Metab*. 2017;37(10):3433-3445. doi:10.1177/0271678X17691056
24. Greenberg SM, Salman RAS, Biessels GJ, et al. Outcome markers for clinical trials in cerebral amyloid angiopathy. *Lancet Neurol*. 2014;13(4):419-428. doi:10.1016/S1474-4422(14)70003-1
25. Zhang Y, Brady M, Smith S. Segmentation of brain MR images through a hidden Markov random field model and the expectation-maximization algorithm. *IEEE Trans Med Imaging*. 2001;20(1):45-57. doi:10.1109/42.906424
26. Greve DN, Fischl B. Accurate and robust brain image alignment using boundary-based registration. *Neuroimage*. 2009;48(1):63-72. doi:10.1016/j.neuroimage.2009.06.060
27. Jenkinson M, Bannister P, Brady M, Smith S. Improved optimization for the robust and accurate linear registration and motion correction of brain images. *Neuroimage*. 2002;17(2):825-841. doi:10.1006/nimg.2002.1132
28. Jenkinson M, Smith S. A global optimisation method for robust affine registration of brain images. *Med Image Anal*. 2001;5(2):143-156. doi:10.1016/S1361-8415(01)00036-6
29. Andersson JL, Jenkinson M, Smith S. *Non-linear registration, aka spatial normalisation*. FMRIB technical report TR07JA2, 2010.
30. Smith SM. Fast robust automated brain extraction. *Hum Brain Mapp*. 2002;17(3):143-155. doi:10.1002/hbm.10062
31. Beckmann CF, Smith SM. Probabilistic independent component analysis for functional magnetic resonance imaging. *IEEE Trans Med Imaging*. 2004;23(2):137-152. doi:10.1109/TMI.2003.822821
32. Woolrich MW, Ripley BD, Brady M, Smith SM. Temporal autocorrelation in univariate linear modeling of FMRI data. *Neuroimage*. 2001;14(6):1370-1386. doi:10.1006/nimg.2001.0931
33. Amunts K, Malikovic A, Mohlberg H, Schormann T, Zilles K. Brodmann's areas 17 and 18 brought into stereotaxic space-where and how variable? *Neuroimage*. 2000;11(1):66-84. doi:10.1006/nimg.1999.0516
34. Fischl B. FreeSurfer. *Neuroimage*. 2012;62(2):774-781. doi:10.1016/j.neuroimage.2012.01.021
35. Coppens EM, Grond J, Hafkemeijer A, Barkey Wolf JJH, Roos RAC. Structural and functional changes of the visual cortex in early Huntington's disease. *Hum Brain Mapp*. 2018;39(12):4776-4786. doi:10.1002/hbm.24322
36. Woolrich MW, Behrens TE, Smith SM. Constrained linear basis sets for HRF modelling using variational Bayes. *Neuroimage*. 2004;21(4):1748-1761. doi:10.1016/j.neuroimage.2003.12.024
37. Bonar DC, Schaper KA, Anderson JR, Rottenberg DA, Strother SC. Graphical analysis of MR feature space for measurement of CSF, gray-matter, and white-matter volumes. *J Comput Assist Tomogr*. 1993;17(3):461-470. doi:10.1097/00004728-199305000-00024
38. Koo TK, Li MY. A guideline of selecting and reporting intraclass correlation coefficients for reliability research. *J Chiropr Med*. 2016;15(2):155-163. doi:10.1016/j.jcm.2016.02.012
39. Birn RM, Smith MA, Jones TB, Bandettini PA. The respiration response function: the temporal dynamics of fMRI signal fluctuations related to changes in respiration. *Neuroimage*. 2008;40(2):644-654. doi:10.1016/j.neuroimage.2007.11.059
40. Chang C, Cunningham JP, Glover GH. Influence of heart rate on the BOLD signal: the cardiac response function. *Neuroimage*. 2009;44(3):857-869. doi:10.1016/j.neuroimage.2008.09.029
41. Bornebroek M, Maat-Schieman MLC, Duinen SGV, Roos RAC. Hereditary cerebral hemorrhage with amyloidosis-Dutch type (HCHWA-D): I - a review of clinical, radiologic and genetic aspects. *Brain Pathol*. 1996;6(2):111-114. doi:10.1111/j.1750-3639.1996.tb00793.x
42. Maat-Schieman ML, Bornebroek M, Haan J, Roos RAC. Hereditary cerebral hemorrhage with amyloidosis-Dutch type (HCHWA-D): II - a review of histopathological aspects. *Brain Pathol*. 1996;6(2):115-120. doi:10.1111/j.1750-3639.1996.tb00794.x
43. Switzer AR, Cheema I, McCreary CR, et al. Cerebrovascular reactivity in cerebral amyloid angiopathy, Alzheimer disease, and mild cognitive impairment. *Neurology*. 2020;95(10):e1333-e1340. doi:10.1212/WNL.00000000000010201
44. Huneau C, Houot M, Joutel A, et al. Altered dynamics of neurovascular coupling in CADASIL. *Ann Clin Transl Neurol*. 2018;5(7):788-802. doi:10.1002/acn3.574

SUPPORTING INFORMATION

Additional supporting information can be found online in the Supporting Information section at the end of this article.

How to cite this article: van Harten TW, van Rooden S, Koemans EA, et al. Impact of region of interest definition on visual stimulation-based cerebral vascular reactivity functional MRI with a special focus on applications in cerebral amyloid angiopathy. *NMR in Biomedicine*. 2023;36(7):e4916. doi:10.1002/nbm.4916